A size-structured food-web model for the global ocean*

Ben A. Ward, Stephanie Dutkiewicz, Oliver Jahn and Mick J. Follows

The MIT Joint Program on the Science and Policy of Global Change combines cutting-edge scientific research with independent policy analysis to provide a solid foundation for the public and private decisions needed to mitigate and adapt to unavoidable global environmental changes. Being data-driven, the Program uses extensive Earth system and economic data and models to produce quantitative analysis and predictions of the risks of climate change and the challenges of limiting human influence on the environment—essential knowledge for the international dialogue toward a global response to climate change.

To this end, the Program brings together an interdisciplinary group from two established MIT research centers: the Center for Global Change Science (CGCS) and the Center for Energy and Environmental Policy Research (CEEPR). These two centers—along with collaborators from the Marine Biology Laboratory (MBL) at Woods Hole and short- and long-term visitors—provide the united vision needed to solve global challenges.

At the heart of much of the Program's work lies MIT's Integrated Global System Model. Through this integrated model, the Program seeks to: discover new interactions among natural and human climate system components; objectively assess uncertainty in economic and climate projections; critically and quantitatively analyze environmental management and policy proposals; understand complex connections among the many forces that will shape our future; and improve methods to model, monitor and verify greenhouse gas emissions and climatic impacts.

This reprint is one of a series intended to communicate research results and improve public understanding of global environment and energy challenges, thereby contributing to informed debate about climate change and the economic and social implications of policy alternatives.

Ronald G. Prinn and John M. Reilly,
Program Co-Directors

For more information, contact the Program office:

MIT Joint Program on the Science and Policy of Global Change
Postal Address:
Massachusetts Institute of Technology
77 Massachusetts Avenue, E19-411
Cambridge, MA 02139 (USA)
Location:
Building E19, Room 411
400 Main Street, Cambridge
Access:
Tel: (617) 253-7492
Fax: (617) 253-9845
Email: ***globalchange@mit.edu***
Website: ***http://globalchange.mit.edu/***

A size-structured food-web model for the global ocean

B. A. Ward,[a,1,*] S. Dutkiewicz,[a] O. Jahn,[a] and M. J. Follows [a]

[a] Massachusetts Institute of Technology, Cambridge, Massachusetts

Abstract

   We present a model of diverse phytoplankton and zooplankton populations embedded in a global ocean circulation model. Physiological and ecological traits of the organisms are constrained by relationships with cell size. The model qualitatively reproduces global distributions of nutrients, biomass, and primary productivity, and captures the power-law relationship between cell size and numerical density, which has realistic slopes of between −1.3 and −0.8. We use the model to explore the global structure of marine ecosystems, highlighting the importance of both nutrient and grazer controls. The model suggests that zooplankton:phytoplankton (Z:P) biomass ratios may vary from an order of 0.1 in the oligotrophic gyres to an order of 10 in upwelling and high-latitude regions. Global estimates of the strength of bottom-up and top-down controls within plankton size classes suggest that these large-scale gradients in Z:P ratios are driven by a shift from strong bottom-up, nutrient limitation in the oligotrophic gyres to the dominance of top-down, grazing controls in more productive regions.

   The size structure of phytoplankton communities is an important determinant of marine ecological function and biogeochemical cycling. Whereas the biomass produced by small phytoplankton is rapidly recycled in the microbial loop at the ocean surface, larger cells sink more rapidly, transporting carbon to the deep ocean and driving the biological carbon pump. Phytoplankton communities that are dominated by large cells are also thought to be associated with short, direct food chains that support large fish populations. These features of marine communities, together with the strong empirical relationships that are found between physiological traits and organism size (Litchman et al. 2007), have motivated the development of marine ecosystem and biogeochemistry models towards the explicit representation of phytoplankton size classes (Moloney and Field 1991; Baird and Suthers 2007; Banas 2011).

   The biogeochemical and ecological functions of marine ecosystems are also affected by taxonomic diversity. Different taxa are often associated with different elemental composition and biogeochemical roles, and recent models have begun to include many different functional groups, in an attempt to capture the taxonomic and biogeochemical diversity of marine communities (reviewed by Hood et al. 2006).

   The interaction of these factors gives rise to a clear global biogeography. Low nutrient regions are dominated by small phytoplankton, such as *Prochlorococcus*, *Synechococcus*, and picoeukaryotes, whereas more productive regions support not only these small cells, but also an additional abundance of larger species, including the coccolithophores, diatoms, and dinoflagellates. These patterns have been observed at local (Schartau et al. 2010), regional (Raimbault et al. 1988), and global scales (Hirata et al. 2011). The large-scale size distribution is so pronounced that its global signature has been detected from space (Kostadinov et al. 2009).

   This pattern of size–class superposition occurs because the amount of phytoplankton biomass in each size class appears to be limited (Chisholm 1992), and total biomass is typically distributed fairly evenly among logarithmically spaced size classes (Sheldon et al. 1972; Chisholm 1992). This leads to a power-law relationship between phytoplankton size and numerical abundance that is ubiquitous throughout the global ocean (Kostadinov et al. 2009). The exponent, or slope, of this relationship is typically found to lie between −1.5 and −0.75 (Cavender-Bares et al. 2001; Cermeño et al. 2006), but in general it is thought to become less steep (i.e., less negative) as total biomass increases and larger cells become established (Kostadinov et al. 2009).

   Figure 1 shows the relationship between phytoplankton size, numerical abundance, and total phytoplankton biovolume in the eastern equatorial Pacific, observed during the IronEx II iron fertilization experiment (Schartau et al. 2010). The dashed and solid lines correspond to measurements taken inside and outside a mesoscale patch of water in which a phytoplankton bloom was stimulated by the addition of dissolved iron. The slope of the power-law relationship changes with total phytoplankton abundance, becoming less negative inside the iron-fertilized patch, as the abundance of large cells increases in relation to small cells.

   What mechanisms dictate this size structuring of marine communities? Empirical observations and theoretical considerations reveal that the physiological rates and ecological interactions of plankton are strongly correlated with organism size. For example, small phytoplankton typically have higher light and nutrient affinities than larger phytoplankton (Finkel 2001; Litchman et al. 2007), and smaller cells are also known to have the largest maximum growth rates, at least within taxonomic groups (Tang 1995). The relationships between phytoplankton size and community structure have previously been explored in numerical models. These range in complexity from zero-dimensional models (Laws 1975; Armstrong 1994; Banas 2011), to more complex regional studies (Moloney and Field 1991; Baird and Suthers 2007; Stock et al. 2008). In

---

   * Corresponding author: ben.ward@ens.fr

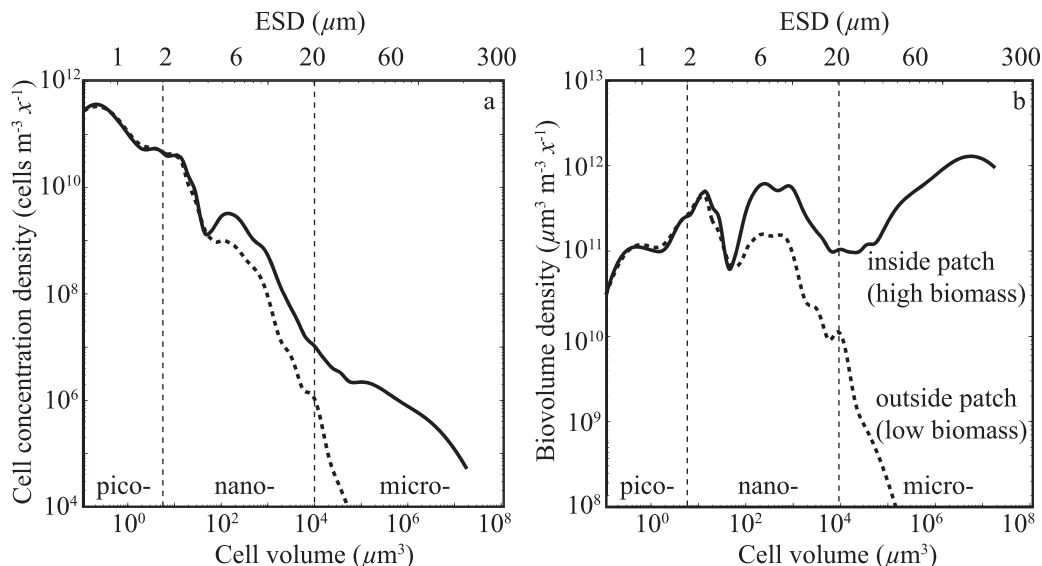   [1] Current address: CERES-ERTI, École Normale Supérieure, Paris, France

Fig. 1.   (a) IronEx II size spectra from Schartau et al. (2010), showing phytoplankton cell concentration density against cell size (volume and ESD). Cell concentration densities outside the iron-fertilized patch are shown with a dashed line. Densities inside the iron-fertilized patch are shown with a solid line. Cell concentration densities are given in units of cells per unit water volume per unit interval along a logarithmic size axis (cells m^{-3} x^{-1}, where x is a dimensionless size variable ($x = \ln[\text{Volume}/V_0] = \ln[\text{Volume}/1 \ \mu m^3]$), and hence "concentration density" is not redundant (Armstrong 2003; Schartau et al. 2010). (b) The corresponding biovolume distribution ($\mu m^3 \ m^{-3} \ x^{-1}$), as a proxy for biomass, is estimated by multiplying cell concentration density by cell volume, assuming spherical cells.

this paper we present a global, size-based model of marine plankton ecology that is embedded within a model of ocean circulation and biogeochemistry. The model begins to resolve the internal cellular physiology of a diverse plankton community, and emphasizes how plankton physiology and ecology underpin observed global biogeography and biogeochemistry. The model qualitatively reproduces observed global patterns of surface nutrients and chlorophyll biomass, and is consistent with empirical estimates of global primary productivity and phytoplankton size fractionation. We use the model to explore the relationships between physiology, ecology, and large-scale community structure, highlighting the role of both bottom-up, nutrient controls, and top-down, grazer controls, in determining the size structure of marine communities.

Methods

The ecosystem model is embedded in a coarse-resolution ($1° \times 1°$ horizontally, 24 vertical levels), climatologically averaged, global ocean circulation model that has been constrained with satellite and in situ observations (Wunsch and Heimbach 2007). The physical model transports 25 size classes of phytoplankton and 30 size classes of zooplankton, as well as inorganic and organic forms of carbon, nitrogen, and iron (phosphate and silicate are not yet included). The phytoplankton state variables are divided into four functional groups, namely analogs of *Prochlorococcus*; picoeukaryotes and *Synechococcus*; small eukaryotes; and large eukaryotes (including diatoms). The model structure is shown schematically in Fig. 2, and the model equations are presented in full in the Web Appendix (www.aslo.orglo/toc/vol_57/issue_6/1877a.pdf).

Biogeochemical and biological tracers interact through the formation, transformation, and remineralization of organic matter. Inorganic nutrients are taken up by phytoplankton, and these are grazed by zooplankton. Mortality, sloppy feeding, and egestion transfer living organic material into sinking particulate and dissolved organic detritus. These are returned to inorganic form through a simple parameterization of bacterial remineralization. The time-dependent change in the biomass of each of the modeled plankton types is described in terms of growth, sinking, grazing, and other mortality, alongside transport and mixing by the fluid flow. Growth itself is a light- (in the case of phytoplankton) and temperature-dependent function of intracellular nutrient reserves, or cell quotas (Droop 1968; Geider et al. 1998). Iron chemistry includes explicit complexation with an organic ligand, scavenging by particles, and representation of aeolian and sedimentary sources (Dutkiewicz et al. 2012).

Complex ecosystem models often require a large number of uncertain empirical parameters to describe the interactions between state variables. Here, following previous work (Moloney and Field 1991; Baird and Suthers 2007), we reduce the number of model parameters by using published power-law functions that link cell volume to physiological traits such as nutrient uptake, quota size, growth, mortality, sinking, and grazing rates. The use of these allometric relationships, and ecological rules governing predator–prey interaction, substantially reduces the number of free parameters.

Phytoplankton physiology—Size-dependent cellular physiology is represented with a quota-based model (Droop 1968). Phytoplankton cells take up nitrate, nitrite, ammo-
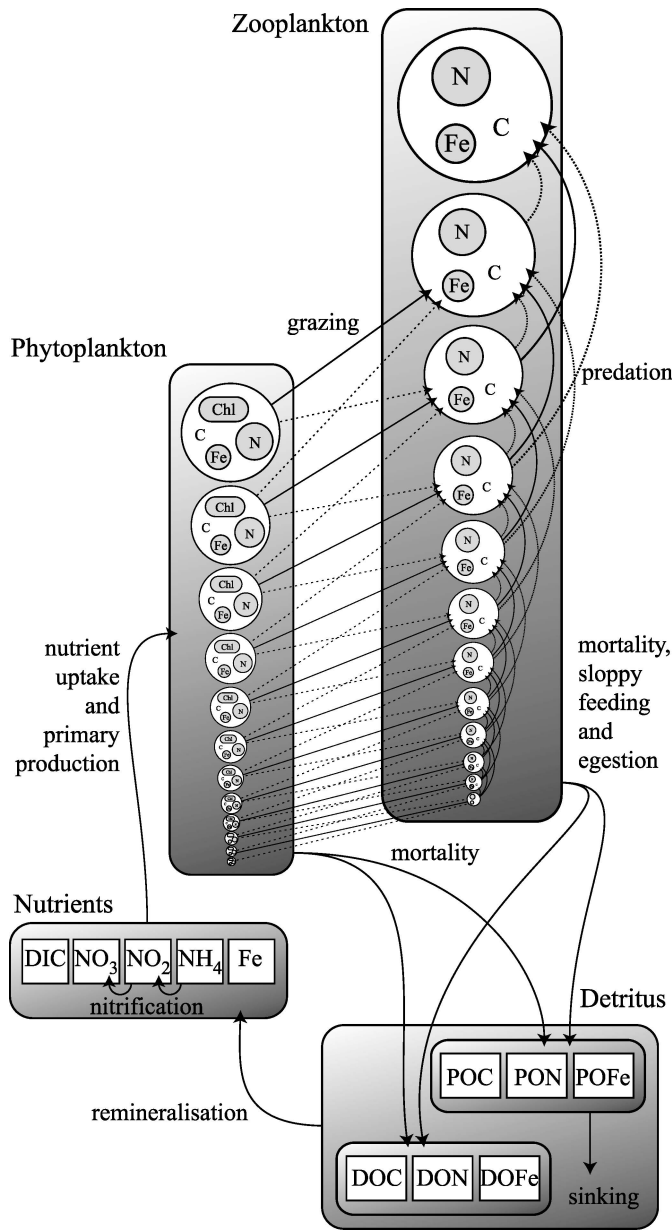
Fig. 2. Schematic representation of the ecosystem model. Not all size classes and not all predator–prey interactions are shown.

The light-limited rate of photosynthetic carbon fixation is calculated as a Poisson function of irradiance (I), modified by the photosynthetic efficiency and the chlorophyll *a* (Chl *a*) : carbon ratio (Q_{Chl}). Chl *a* synthesis is regulated as phytoplankton attempt to match the level of light harvesting to the maximum rate at which photons can be utilized for carbon fixation (Geider et al. 1998). Depending on this ratio, a certain fraction of newly assimilated nitrogen is diverted to the synthesis of Chl *a*. Chl *a* synthesis is tightly coupled to new nitrogen assimilation because of the high demand for nitrogen in the apoprotein of the photosynthetic pigment–protein complex, and because the intracellular mobilization of nitrate, ammonium, and amino acid pools is assumed to be negligible in this process (Geider et al. 1998). Phytoplankton rate processes are modified using a single Arrhenius-like temperature-dependence function (Dutkiewicz et al. 2012).

Grazing and predation—For the sake of brevity, we use the term "predator" to describe any zooplankton type, regardless of whether it feeds on zooplankton, phytoplankton, or some combination of both. We use the term "prey" to describe any food type, including both phytoplankton and zooplankton.

Grazing rates within the zooplankton community are calculated as a function of prey carbon concentrations using a sigmoidal functional response. Grazing pressure is reduced at low overall prey concentrations, and saturates to a maximum rate at high prey concentrations. Grazing rates are modified by the same Arrhenius-like temperature function that is used for phytoplankton (Dutkiewicz et al. 2012).

Zooplankton types do not modify their attack rate according to the density of individual prey types, as this has no empirical justification (Gentleman et al. 2003). They do, however, modify their attack rates between phytoplankton and zooplankton, preferentially feeding on the more dense group. This behavior is adopted following the observation that omnivorous zooplankton may switch to filter feeding in the presence of large amounts of nonmotile phytoplankton prey, but will adopt an ambush feeding mode when the prey field is dominated by motile zooplankton prey. This sort of switching behavior both is empirically justified and has also been shown to increase model stability (Gentleman et al. 2003).

We assume that the probability of a predator–prey encounter decreases with increasing predator–prey length ratio ($\vartheta_{j_{pred}, j_{prey}}$), because smaller prey are harder to detect. The probability of successful ingestion given such an encounter, however, increases with the predator–prey length ratio, because smaller prey are less likely to escape and are easier to ingest. The resultant grazing preference ($\phi_{j_{pred}, j_{prey}}$) thus has a log-normal distribution, which is centered on a predator : prey length ratio of 10 (Kiørboe 2008). The standard deviation of the logarithm of the preferred length ratio is set to 0.5.

Prey assimilation is calculated according to the nutritional demands of the grazer, with assimilation of nitrogen and iron down-regulated according to the size of the predator nutrient quotas. Unassimilated prey biomass is

nium, and iron into internal nitrogen and iron reservoirs, as a function of cell size (*see* "Size-dependent traits") and in accordance with Michaelis-Menten kinetics. The uptake of inorganic carbon by photosynthesis is limited by a lack of light or essential nutrient reserves, following Geider et al. (1998) and Moore et al. (2002). In nutrient-limited situations, photosynthetic carbon fixation is limited by the size of the most depleted quota. In nutrient-replete environments photosynthesis becomes light- and temperature-limited, and nutrient uptake is down-regulated by a linear satiation function as cells approach their maximum capacity. Photosynthetic efficiency is also regulated by the size of the iron quota (Moore et al. 2002).

Table 1. Size-independent biological parameters.

Parameter	Symbol	Value	Units
Nutrient uptake			
Ammonium inhibition	Ψ	4.6*	$(\text{mmol N m}^{-3})^{-1}$
Zooplankton nitrogen quotas			
Minimum nitrogen:carbon quota	Q_N^{min}	0.075	mmol N (mmol C)$^{-1}$
Maximum nitrogen:carbon quota	Q_N^{max}	0.151	mmol N (mmol C)$^{-1}$
Plankton Iron quotas			
Minimum iron:carbon quota	Q_{Fe}^{min}	1.5×10^{-6}	mmol Fe (mmol C)$^{-1}$
Maximum iron:carbon quota	Q_{Fe}^{max}	80.0×10^{-6}	mmol Fe (mmol C)$^{-1}$
Temperature			
Reference temperature	T_{ref}	20	°C
Temperature dependence	R	0.05	-
Photosynthesis			
Maximum Chl a:nitrogen ratio	θ_N^{max}	3.0†	mg Chl a (mmol N)$^{-1}$
Initial slope photosynthesis–irradiance curve	α	3.83×10^{-7}†	mmol C (mg Chl a)$^{-1}$(μEin m^{-2})$^{-1}$
Cost of biosynthesis	ξ	2.33†	mmol C (mmol N)$^{-1}$
Grazing			
Optimum predator:prey radius ratio	ϑ_{opt}	10‡	-
Standard deviation of log of preference	σ_{graz}	0.5	-
Total prey half-saturation	k_C^{prey}	1.0	mmol C m^{-3}
Maximum assimilation efficiency	λ^{max}	0.7	-
Prey refuge parameter	Λ	−1.0	-
Mortality			
Linear plankton mortality	m_p	0.02	d^{-1}

* Dutkiewicz et al. 2012.
† Geider et al. 1998.
‡ Kiørboe 2008.

passed directly to organic matter. To avoid excessive accumulation of carbon when feeding on low-quality prey (i.e., high carbon:nutrient ratios), carbon assimilation is reduced in proportion to the most depleted of the grazer's N and Fe quotas. If both these quotas are full, C is assimilated at the maximum rate. If either is empty, C assimilation is down-regulated until sufficient quantities of the limiting element are acquired.

Recycling of organic matter—Dissolved and particulate organic matter pools (DOM and POM) are produced by plankton mortality and unassimilated feeding. DOM does not sink, whereas POM is parameterized to sink at a rate of 10 m d^{-1} (Dutkiewicz et al. 2012). The fractions of biomass that are passed to DOM and POM are assigned on the basis of taxonomic group. Organic matter produced by mortality of, and feeding on, *Prochlorococcus*, *Synechococcus*, and picoeukaryotes is divided 80:20 between DOM and POM, allowing strong recycling within the microbial loop. Organic matter produced by losses from the small eukaryotes, large eukaryotes, and zooplankton is split 50:50, allowing faster sinking and export from the euphotic zone. We do not resolve heterotrophic bacteria, but parameterize the remineralization of organic matter as a constant linear rate.

Size-dependent traits—The model is parameterized using physiological and ecological relationships drawn from the literature. Some parameters, such as the linear mortality rate, are size independent, and a single value is assigned to all plankton (Table 1). Other, size-dependent parameters, such as the maximum uptake rate for nitrate, are set as a function of cell volume:

$$p = aV^b \qquad (1)$$

Here p is a parameter value for a cell of volume V, and b is an exponent describing the size dependence. In most cases a is assigned a constant value for all groups, indicating that all groups are described with a single power-law relationship (Table 2). This was not appropriate for the maximum photosynthetic rate, which also varies by taxonomic group (Raven 1998; Litchman et al. 2007). We therefore apply a separate value of a for each plankton group (Table 3), so that within groups, larger cells have slower growth rates, but among cells of similar size, diatoms will have the fastest growth rates, and *Prochlorococcus* will have the slowest (Fig. 3). This approach was taken following Irwin et al. (2006). Raven (1998) argued that maximum growth rates decrease in smaller taxa because these must assign more of the limited space within the cell to non-scalable cellular machinery, such as the genome and the cell membrane.

The maximum grazing rate is set according to allometric relationships defined by Hansen et al. (1997) (Table 2). The effective half-saturation constant for

Table 2. Size-dependent biological parameters and scaling coefficients ($a\mathrm{V}^b$).

Parameter	Symbol	a	b	Parameter units
Inorganic nutrient uptake				
Maximum uptake rate	$V_{NO_3}^{max}$	0.51‡	−0.27‡	mmol N (mmol C)$^{-1}$ d^{-1}
	$V_{NO_2}^{max}$	0.51	−0.27	mmol N (mmol C)$^{-1}$ d^{-1}
	$V_{NH_4}^{max}$	0.26	−0.27	mmol N (mmol C)$^{-1}$ d^{-1}
	V_{Fe}^{max}	14.0×10^{-6}*	−0.27	mmol Fe (mmol C)$^{-1}$ d^{-1}
Half-saturation concentration	k_{NO_3}	0.17‡†	0.27‡†	mmol N m^{-3}
	k_{NO_2}	0.17	0.27	mmol N m^{-3}
	k_{NH_4}	0.085	0.27	mmol N m^{-3}
	k_{Fe}	80.0×10^{-6}*	0.27	mmol Fe m^{-3}
Plankton cellular carbon quotas				
Cell carbon content	Q_C	18.0×10^{-12}†	0.94†	mmol C cell^{-1}
Phytoplankton nitrogen quotas				
Minimum nitrogen : carbon quota	Q_N^{min}	0.07‡†	−0.17‡†	mmol N (mmol C)$^{-1}$
Maximum nitrogen : carbon quota	Q_N^{max}	0.25§†	−0.13§†	mmol N (mmol C)$^{-1}$
Photosynthesis				
Maximum photosynthesis at T=T_{ref}	P_C^{max}	*See* Table 3	−0.15‖	d^{-1}
Grazing				
Maximum prey ingestion rate	G_C^{max}	21.9¶	−0.16¶	d^{-1}
Sinking				
Phytoplankton sinking rate	w_p	0.28#	0.39#	m d^{-1}

* Mongin et al. 2006.
† Menden-Deuer and Lessard 2000.
‡ Litchman et al. 2007.
§ Montagnes and Franklin 2001.
‖ Tang 1995.
¶ Hansen et al. 1997.
# Laws 1975.

grazing is set to 1 mmol C m^{-3}. This is smaller than typical experimental estimates (Hansen et al. 1997), but the use of prey-preference terms in the multi-prey functional response makes comparison with observations difficult at best (Banas 2011). We also note that high grazing pressure is required to compensate for the omission of density-dependent viral lysis, which is known to be an important source of microbial mortality (Suttle 2007).

The remaining model parameters are assigned values based on allometric or non-allometric physiology, as listed in Tables 1–4.

Results

The model is initialized with each phytoplankton and zooplankton class assigned a low biomass of 1×10^{-9} mmol C m^{-3}, 1.51×10^{-10} mmol N m^{-3}, and 6.66×10^{-15} mmol Fe m^{-3} (a C : N : Fe ratio of $106:16:0.7 \times 10^{-3}$). Phytoplankton are assigned an initial chlorophyll biomass of 6.28×10^{-10} mg Chl m^{-3}. Dissolved inorganic pools of carbon and nitrate are initialized from climatological data (Conkright et al. 2002). Initial distributions of nitrite, ammonium, and iron are taken from the model of Dutkiewicz et al. (2012). The model is integrated forwards for 30 yr with a biological time step of 30 min. Tracers are advected with a time step of 1 h.

After approximately 20 yr of integration, bulk properties such as total phytoplankton and zooplankton biomass settle into a repeating seasonal cycle, albeit with small, possibly chaotic, interannual variation within individual size classes. This instability may be a consequence of the highly complex model food web, and may reflect the chaotic instability of natural systems (Banas 2011). The presented model results are nonetheless robust in their characteristics across the final 5 yr of integration. All results that are shown are taken from the final year of integration.

Global biomass and productivity—Model estimates of the global annual mean surface NO$_3$, chlorophyll, and depth-integrated primary production are shown in comparison to empirically derived estimates in Fig. 4. The model qualita-

Table 3. Group-specific coefficients for maximum photosynthesis at T = T_{ref} ($P_C^{max} = a\mathrm{V}^{-0.15}$), following Irwin et al. (2006), and fractionation of organic matter production.

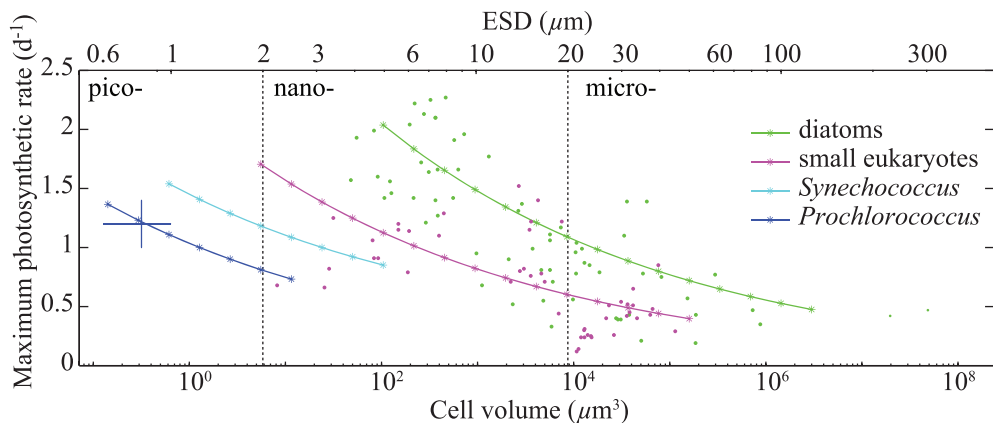| Phytoplankton functional type	a	β^{mort}	β^{graz}
Diatoms	3.8	0.5	0.5
Other eukaryotes	2.1	0.5	0.5
Synechococcus	1.4	0.8	0.8
Prochlorococcus	1.0	0.8	0.8

Fig. 3. Maximum phytoplankton growth rates as a function of cell size (volume and ESD) and taxon. Small dots represent experimental estimates of maximum growth rates, taken from Tang (1995). Blue error bars give estimated size and growth rates for *Prochlorococcus* (Irwin et al. 2006). The stars represent the growth rates of the 50 modeled phytoplankton types.

tively captures the large-scale global NO_3 and chlorophyll distributions, with low nutrients and biomass in the subtropical gyres, and higher nutrients and biomass in subpolar regions. The North Atlantic correctly shows intermediate nutrient concentrations and high biomass, and the high-nutrient, low-chlorophyll regions of the North Pacific, equatorial Pacific, and Southern Ocean are also captured.

Chlorophyll biomass and primary productivity are underestimated in the centers of the subtropical gyres. This could be related to the omission of certain phytoplankton traits that are well suited to oligotrophic environments, such as nitrogen fixation and mixotrophy. Additionally, the coarse resolution of the physical model, which does not resolve eddies, omits an important nutrient flux into the oligotrophic ocean surface. Chlorophyll biomass is also underestimated in coastal regions. Although satellite estimates of chlorophyll may be unreliable in these areas, as a consequence of high levels of particulate matter, much of the model shortfall may again be attributed to the physical model, in which coastal processes are poorly resolved. The modeled global primary production is 35 Gt C yr^{-1}, which is at the low end of satellite-derived estimates (35–70 Gt C yr^{-1}, Carr et al. 2006).

Table 4. Biogeochemical parameters, values, and units.*

Parameter	Symbol	Value	units
Inorganic nitrogen			
Ammonium to nitrite oxidation rate	ζ_{NH_4}	2[†]	d^{-1}
Nitrite to nitrate oxidation rate	ζ_{NO_2}	0.1[†]	d^{-1}
Upper PAR threshold for nitrification	I_{Ox}	10[†]	μEin m^{-2} s^{-1}
Iron			
Iron scavenging rate	c_{scav}	4.4×10^{-3}	d^{-1}
Particulate organic matter			
POC remineralization rate	r_{POC}	0.04	d^{-1}
PON remineralization rate	r_{PON}	0.04	d^{-1}
POFe remineralization rate	r_{POFe}	0.04	d^{-1}
POM sinking rate	w_{POM}	10[†]	m d^{-1}
Dissolved organic matter			
DOC remineralization rate	r_{DOC}	0.02[†]	d^{-1}
DON remineralization rate	r_{DON}	0.02[†]	d^{-1}
DOFe remineralization rate	r_{DOFe}	0.02[†]	d^{-1}
DOM sinking rate	w_{DOM}	0	m d^{-1}
Light attenuation			
Light attenuation by water	k_w	0.04[†]	m^{-1}
Light attenuation by chlorophyll	k_{Chl}	0.03[‡]	m^{-1} (mg Chl) $^{-1}$

* PAR = Photosynthetically Available Radiation; POC = Particulate Organic Carbon; PON = Particulate Organic Nitrogen; POFe = Particulate Organic Iron; DOC = Dissolved Organic Carbon; DON = Dissolved Organic Nitrogen; DOFe = Dissolved Organic Iron.
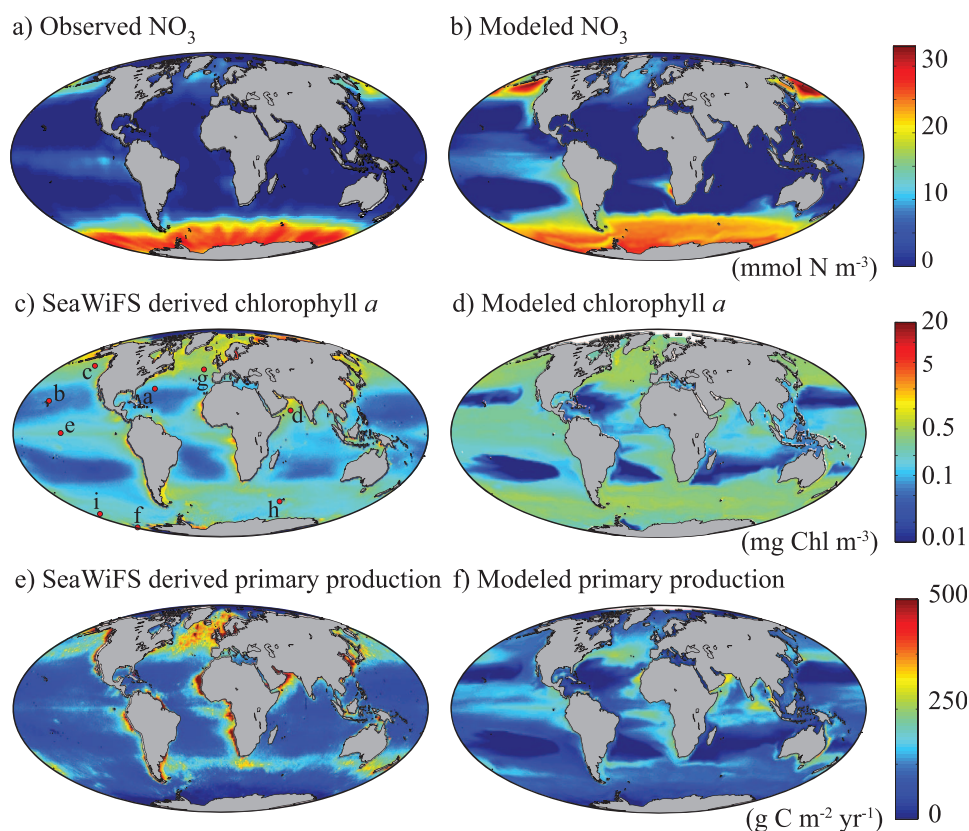† Dutkiewicz et al. 2012.
‡ Moore et al. 2002.

Fig. 4. Observed and model fields of global NO$_3$, chlorophyll, and primary production. (a) Climatological surface NO$_3$ (mmol N m^{-3}) from Conkright et al. (2002). (b) Model annual mean surface NO$_3$ (mmol N m^{-3}). (c) Sea-viewing Wide Field-of-view Sensor (SeaWiFS) annual composite chlorophyll (mg Chl m^{-3}), with the location of nine JGOFS sites (*see* Fig. 6) shown: a, BATS; b, HOT; c, Station P; d, Arabian Sea; e, equatorial Pacific; f, Ross Sea; g, NABE; h, Kerfix; i, Polar Front. (d) Model annual mean surface Chl *a* (mg Chl *a* m^{-3}). (e) SeaWiFS derived estimate of annual mean primary production (mg C m^{-3} d^{-1}) (Behrenfeld and Falkowski, 1997). (f) Model annual mean surface primary production (mg C m^{-3} d^{-1}).

The modeled distributions of depth-integrated phytoplankton and zooplankton carbon biomass are shown in Fig. 5a,b. As expected, regions of high phytoplankton and zooplankton abundance are concentrated in subpolar and coastal regions, whereas the oligotrophic gyres support much lower total biomass. Figure 5c shows the distribution of the depth-integrated zooplankton : phytoplankton (Z : P) ratio. This indicates a shift from low Z : P ratios in the open ocean to high Z : P ratios in coastal areas. This result is qualitatively consistent with observations collated by Gasol et al. (1997), who found an average Z : P ratio of 0.51 ± 0.05 in the open ocean, increasing to 0.87 ± 0.18 in coastal regions. For comparison, Taylor et al. (2011) found an average Z : P ratio of 0.78 ± 0.17 in the equatorial Pacific.

Seasonal cycle—The seasonal cycle of chlorophyll in the surface mixed layer is compared to in situ observations from nine Joint Global Ocean Flux Study (JGOFS) time-series sites (Kleypas and Doney 2001) in Fig. 6. Mixed-layer chlorophyll concentrations were available from Bermuda Atlantic Time-series Study (BATS; 64°W, 32°N), Hawaii Ocean Time-series (HOT; 158°W, 23°N),

Station P (145°W, 50°N), Arabian Sea (62°E, 16°N), equatorial Pacific (140°W, 0°N), Ross Sea (180°W, 76°S), North Atlantic Bloom Experiment (NABE; 19°W, 47°N), Kerfix (68°E, 51°S), and Polar Front (170°W, 62°S).

The observed seasonal cycle in mixed-layer chlorophyll concentration is captured reasonably well at all sites, with the exception of HOT. We attribute the failure of the model at this site to the omission of nitrogen fixation and the lack of explicitly resolved eddies. We also note that although the model underestimates the chlorophyll concentration by a factor of two at HOT, this only amounts to between 0.05 and 0.1 mg Chl m^{-3} in absolute terms.

The observations show greater short-term variability than the model at a number of sites. The observations at most sites are comprised of data from several different years, and therefore reflect interannual variability in the timing and magnitude of blooms and storm events. These are not captured in this coarse-resolution model, which is forced by a single year of climatological data. The chlorophyll biomass within each phytoplankton size class is shown cumulatively in Fig. 6. We note that individual size classes generally have very low biomass, even during blooms.
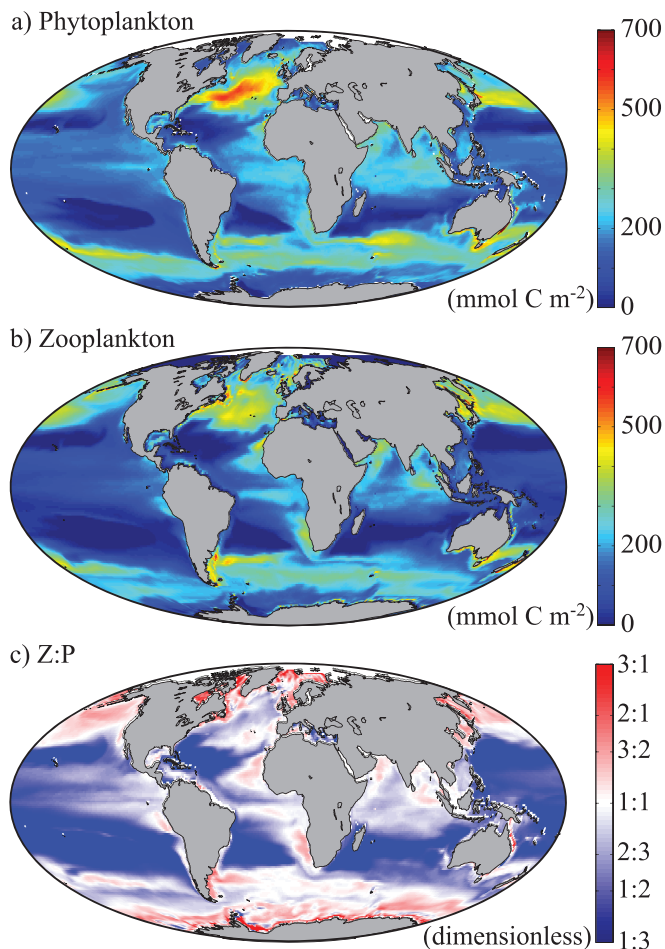
a) Phytoplankton

b) Zooplankton

c) Z:P

Fig. 5. Depth integrated carbon biomass for (a) phytoplankton (mmol C m^{-2}) and (b) zooplankton (mmol C m^{-2}); (c) shows the ratio of depth-integrated zooplankton to phytoplankton biomass.

Biodiversity and ecosystem composition—Estimates of the biomass within three approximately size-based phytoplankton groups, based on satellite estimates of chlorophyll, and empirical relationships between total chlorophyll biomass and phytoplankton accessory pigments, are shown in Fig. 7a,c,e (Hirata et al. 2011). The three groups correspond approximately to the picophytoplankton (diameter $\leq 2~\mu m$), nanophytoplankton ($2 \leq$ diameter $< 20~\mu m$) and microphytoplankton (diameter $> 20~\mu m$) size classes. Figure 7b,d,f shows model estimates of similar phytoplankton groups (note that there are differences in classification between the modeled and observed groups; for instance, some observed groups, such as prymnesiophytes and dinoflagellates, are not explicitly resolved in the model).

Empirical estimates of the small picoeukaryotes, prokaryotes, and *Prochlorococcus* are shown in Fig. 7a. These organisms are present at low abundance over almost the entire ocean. They are most abundant in upwelling regions and coastal zones, but their annual average chlorophyll biomass rarely exceeds 0.1 mg Chl m^{-3}. The modeled analogs of *Prochlorococcus* and *Synechococcus* are also widely distributed across the global ocean. Their chlorophyll concentration is consistently higher than the empirical estimates, often approaching 0.2 mg Chl m^{-3}, but we note that there are significant observational errors associated with these satellite-derived estimates (Hirata et al. 2011). The discrepancy may also be attributable to the lack of density-dependent viral mortality in the model (Suttle 2007).

The estimated abundance of the slightly larger prymnesiophytes and green algae are shown in Fig. 7c. These cells are less widespread than the prokaryotes, and are excluded from large areas of the subtropical oceans. Chlorophyll concentrations in this group also rarely exceed 0.1 mg Chl m^{-3},
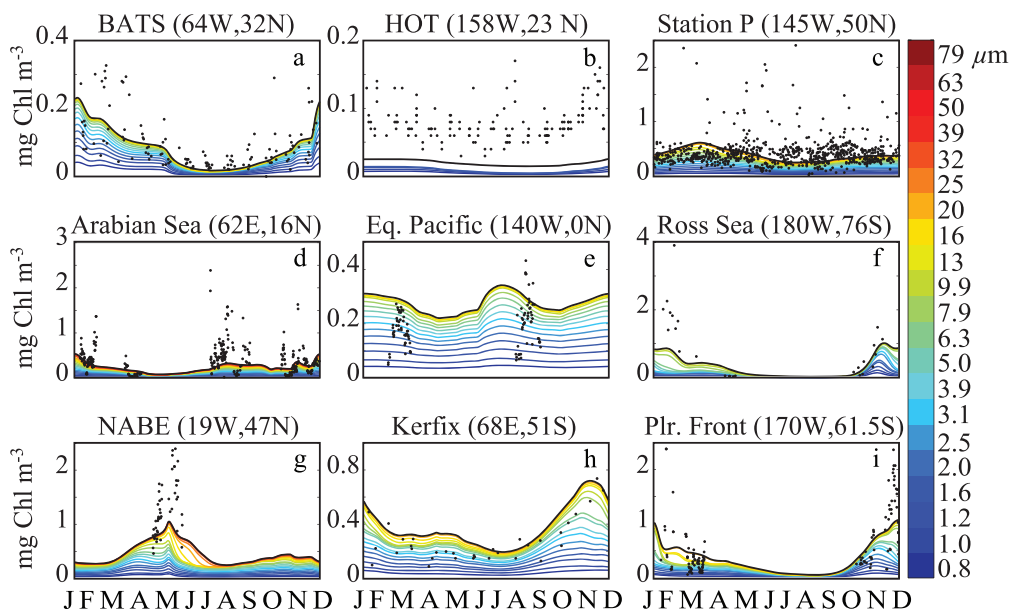

Fig. 6. Seasonal cycle of modeled total mixed-layer chlorophyll concentrations (black lines), with in situ measurements from JGOFS sites (black dots). Note different scales on *y*-axes. The site locations are indicated in Fig. 4. Community composition is shown by dividing the total chlorophyll biomass into constituent size classes, as shown by the distance between colored lines. The cell diameter within each size class is indicated by the color scale. Size classes for which the surface biomass did not once exceed 0.01 mg Chl m^{-3} are not shown.

a) Pico-eukaryotes, prokaryotes and Prochlorococcus

b) Modeled pico-eukaryotes, Synechococcus and Prochlorococcus

c) Prymnesiophytes and green algae

d) Modeled small eukaryotes

e) Diatoms and dinoflagellates
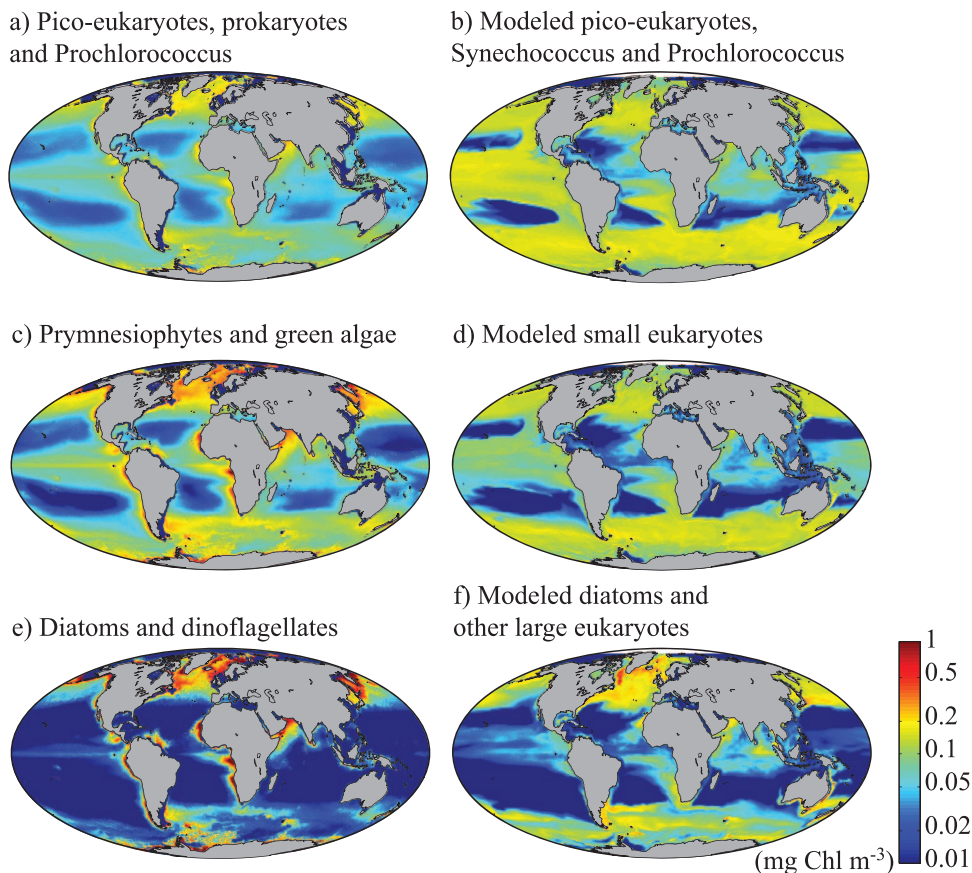
f) Modeled diatoms and other large eukaryotes

Fig. 7. Satellite estimates of surface chlorophyll biomass associated with different taxonomic groups. (a,c,e) Estimated chlorophyll concentrations in three subgroups of phytoplankton: (a) cyanobacteria, prochlorophytes, and green flagellates, (c) cryptophytes, chromophytes, and nanoflagellates, and (e) diatoms and dinoflagellates (Hirata et al. 2011). (b,d,f) Similarly sized model counterparts, namely (b) *Prochlorococcus* and *Synechococcus*, (d) small eukaryotes, and (f) diatoms and other large eukaryotes. Note that there are some differences in classification between the modeled and empirically estimated groups.

except in the North Atlantic and coastal regions. The modeled small eukaryotes are similarly distributed over much of the open ocean.

The estimated chlorophyll biomass of the largest phytoplankton group, consisting of diatoms and dinoflagellates, is shown in Fig. 7e. These groups are restricted to the North Atlantic, coastal and equatorial upwelling regions, and fertile patches in the Southern Ocean, particularly downstream of the southernmost points of South America and Africa. High chlorophyll abundance also occurs around islands such as South Georgia and the Kerguelen and Crozet Islands, where sedimentary iron sources can initiate large phytoplankton blooms (Boyd and Ellwood 2010). The model diatoms and other large eukaryotes are similarly restricted to high latitude and upwelling regions. The blooms of large phytoplankton off the southern tips of South America and Africa also appear in the model, as do the patches of high biomass around remote islands.

Although there are discrepancies between the model and observations, the model successfully captures the overarching trend among the three phytoplankton size classes,

where picophytoplankton make up a widespread background population, and the larger nano- and microphytoplankton coexist alongside them in regions of higher total biomass.

Community size structure—Observations, such as those shown in Fig. 1, reveal a consistent, power-law relationship between phytoplankton size and numerical abundance, that typically becomes less steep with increasing total biomass. We examined the size–abundance relationship in the model by sorting surface grid cells into six logarithmically spaced groups according to the annual mean surface phytoplankton biomass. Within each of these groups, the average cell density (cells m^{-3}) and biomass (mmol C m^{-3}) were calculated for each phytoplankton size class. The log of cell numerical abundance is plotted against the log of cell diameter in Fig. 8a.

The modeled relationship between cell diameter and cell density shown in Fig. 8a is qualitatively consistent with the observations shown in Fig. 1: the numerical abundance of cells in each size classes decreases according to a power-law relationship with cell diameter, and as total phytoplankton
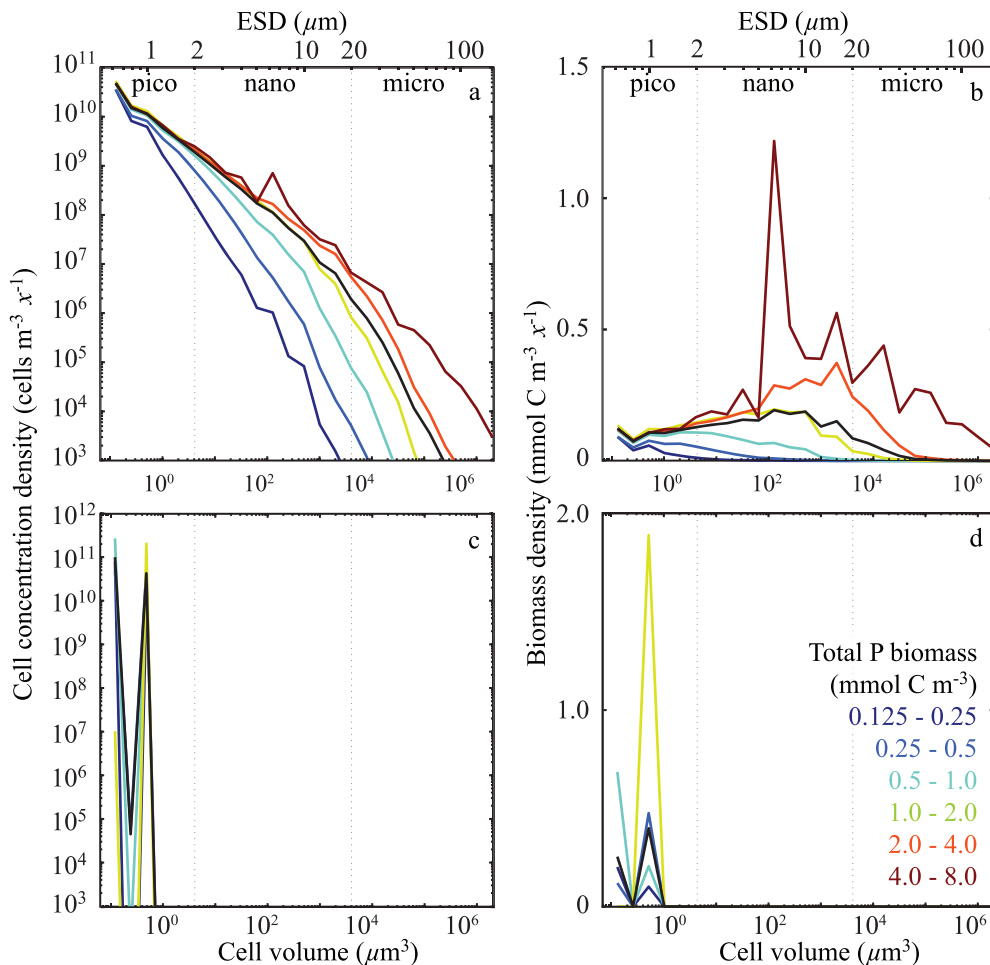
Fig. 8. Modeled surface phytoplankton size spectra as a function of total phytoplankton carbon biomass. Surface grid cells were divided among eight logarithmically spaced bins according to total annual mean phytoplankton carbon biomass. The global average distribution is also shown with a solid black line. Cell concentration and biomass densities are given in units of cell or biomass concentration per unit interval along a logarithmic volume axis (cells m^{-3} x^{-1} and mmol C m^{-3} x^{-1}, where x is a dimensionless size variable ($x = \ln[\text{Volume}/V_0] = \ln[\text{Volume}/1\ \mu\text{m}^3]$). (a) The relationship between log cell volume and log cell concentration density. (b) The relationship between log cell volume and log biomass density. Cell concentrations and biomasses within each size class can be found by multiplying by the size class separation, $x = \ln[2]$. Estimated slopes and intercepts of the phytoplankton size spectra shown in (a) are given in Table 5. (c,d) are equivalent to (a,b), but represent the model run with no size preference for grazing (*see* Discussion).

biomass increases, the abundance of small cells remains relatively constant, whereas the number of large cells increases by several orders of magnitude.

Figures 1, 7, 8a confirm that total phytoplankton biomass increases through the addition of ever larger size classes. This pattern is also apparent in Fig. 8b, which shows phytoplankton carbon biomass as a function of log cell diameter in each of the 6 total biomass groups. As total biomass increases, the biomass within individual size classes begins to saturate, first in the smallest size classes, and then in larger size classes. As a consequence of this saturation, biomass accumulation occurs at the right-hand side of the size distribution, as larger cells become established. This pattern is consistent with global estimates

of phytoplankton size structure based on observations of accessory pigments (Hirata et al. 2011).

In regions where total biomass is less than 2 mmol C m^{-3}, biomass accumulates in a relatively consistent way. Larger size classes accumulate with increasing total biomass, and the size distribution remains fairly smooth across different size classes. Additionally, as larger size classes become established, they are able to support higher biomasses than the smaller size classes. This pattern is likely related to the slower growth rates of larger zooplankton (Armstrong 1994). The smooth relationships between cell size and biomass break down in regions of high biomass (i.e., > 2 mmol C m^{-3}), which are typically associated with transient phytoplankton blooms. The sharp peak in

Table 5. Slopes (*b*) and intercepts (*a*) of the phytoplankton size spectrum (cell concentration density = aV^b), after binning and averaging by total carbon biomass. Cell concentration densities are given in units of cells per unit water volume per unit interval along a logarithmic size axis (cells m^{-3} x^{-1}, where $x = \ln[V/V_0]$).

Carbon biomass (mmol C m^{-3})	a (cells m^{-3} x^{-1})	b
0.125–0.25	1.8×10^9	-1.29
0.25–0.5	3.2×10^9	-1.17
0.5–1.0	6.0×10^9	-1.06
1.0–2.0	8.9×10^9	-0.98
2.0–4.0	8.4×10^9	-0.90
4.0–8.0	8.3×10^9	-0.82
Global average	6.9×10^9	-0.86

abundance of cells at an equivalent spherical diameter (ESD) of 4 μm corresponds to the fastest growing phytoplankton size class (Table 3), which suggests a niche for fast-growing "opportunist" species under bloom conditions.

The relationship between phytoplankton numerical abundance and cell size is often summarized by the slope of the power-law relationship between cell density and cell volume. Modeled phytoplankton spectral slopes were calculated within the six biomass categories, and are shown together with a global estimate in Table 5. Very rare phytoplankton species are infrequently sampled in the real ocean, and their distribution and abundance are poorly understood (Cermeño et al. 2006). We therefore exclude the largest and rarest cells (comprising the last 1% of the total phytoplankton biomass) from the analysis. In this way the average size distribution was calculated only from those size classes showing a power-law relationship between cell size and abundance.

The modeled slopes increase from -1.29, in regions of very low biomass, to -0.86, in regions of very high biomass, within the observed range of approximately -1.5 to -0.75 (Cermeño et al. 2006).

Discussion

The pelagic ecosystem model qualitatively reproduces the observed global distributions of nitrate, chlorophyll, and primary production, and captures the observed size structure of marine communities (Raimbault et al. 1988; Hirata et al. 2011). The ability of the model to reproduce the observed biogeography and community size structure suggests that it provides a suitable framework for further exploration of the mechanisms that underpin these distributions.

Phytoplankton size—Sheldon et al. (1972) noted that particulate biomass is distributed evenly among logarithmically spaced size classes, and hence cell density decreases logarithmically across the same size classes. This size structuring appears to be a consequence of several factors that affect marine phytoplankton communities. Smaller cells have a higher surface area : volume ratio and a faster diffusive nutrient encounter rate than larger cells, and so

have faster nutrient uptake rates (Tang 1995; Litchman et al. 2007). Smaller cells also tend to sink more slowly than large cells. Conversely, large cells may benefit from large storage quotas under both transient and equilibrium conditions, and may be less susceptible to the size-dependent exudation of metabolites (Kriest and Oschlies 2007).

In general, however, the nutritional demands of phytoplankton cells are positively correlated with cell size, and smaller cells are able to survive at lower resource concentrations than large cells. This relationship reveals how increases in nutrient availability may lead to increased coexistence of larger cells (Irwin et al. 2006). In some regions, short-term physical processes (such as convective or tidal mixing) lead to rapid accumulation of nutrients in the surface ocean, allowing for transient blooms of large cells. By contrast, wherever the nutrient supply is relatively constant, small cells should, in theory, always draw nutrients down to very low levels, thereby excluding any larger phytoplankton with higher resource requirements (Armstrong 1994; Irwin et al. 2006). Even in upwelling regions, where nutrient supply rates are very high, the relatively constant supply should allow small phytoplankton to accumulate sufficient biomass to draw nutrients down to very low levels.

In the ocean, large cells are clearly not excluded from regions with high nutrient supply. The observations and model output in Figs. 1, 7, 8 emphasize that biomass is relatively evenly distributed across phytoplankton size classes. Small phytoplankton do not accumulate to very high biomasses, and large phytoplankton are not excluded from regions with constant high supply. How is it that so many large species are able to coexist alongside smaller species, given that these have much lower equilibrium resource requirements?

The fact that biomasses in individual size classes seem to have an upper limit (e.g., Fig. 8) suggests that something other than competition for nutrients is acting to control the abundance of small phytoplankton in regions of high nutrient supply.

Bottom-up and top-down controls—Arguably the most important factor underpinning the diversity and size structure of marine communities is the control of successful populations by zooplankton grazing and viral lysis (Thingstad and Sakshaug 1990; Armstrong 1994). Often referred to as the "kill-the-winner" hypothesis (Thingstad and Lignell 1997), the theory states that the total amount of biomass within any one size class is limited by density-dependent losses. No individual size class can dominate completely, as very high abundances are kept in check by high mortality. In line with these arguments, only the smallest and most competitive phytoplankton are able to survive in regions of very low resource supply. In regions where nutrients are more abundant, grazing pressure and viral lysis prevent the small cells from consuming all resources, and progressively larger cells become established.

The kill-the-winner mechanism also provides an elegant solution to the so-called "paradox of the plankton" (Hutchinson 1961), which asks how so many phytoplank-

a) Picophytoplankton growth limitation   b) Z:P (picophytoplankton and their grazers)

c) Nanophytoplankton growth limitation   d) Z:P (nanophytoplankton and their grazers)

e) Microphytoplankton growth limitation   f) Z:P (microphytoplankton and their grazers)
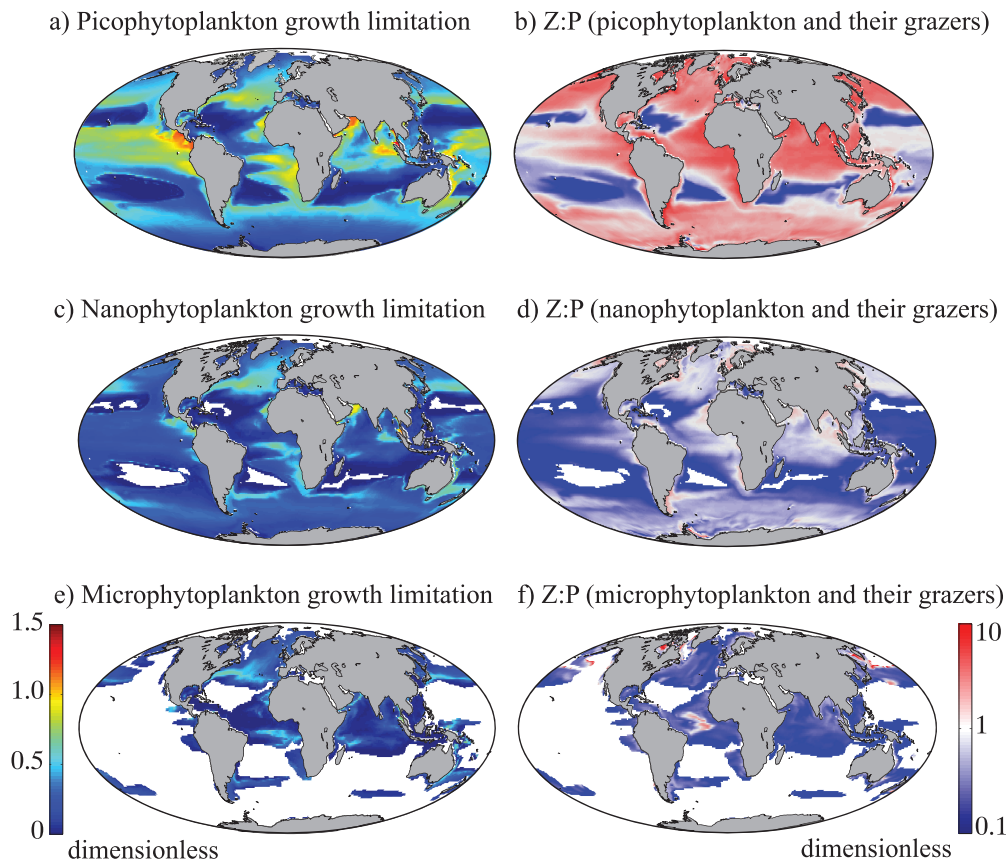

Fig. 9.   Bottom-up and top-down controls in three phytoplankton size classes. The left-hand maps (a,c,e) show the annual average of combined nutrient, light, and temperature limitation at the ocean surface, expressed as a fraction of the maximum growth rate at 20°C. The right-hand maps (b,d,f) show zooplankton to phytoplankton ratios in each size class. (b) Picophytoplankton (< 2 μm) and their grazers (< 20 μm), (d) nanophytoplankton (2–20 μm) and their grazers (20–200 μm), and (f) microphytoplankton (> 20 μm) and their grazers (> 200 μm). Within each size class, areas with surface phytoplankton biomass less than 0.001 mmol C m^{-3} are left blank. Note the logarithmic color scale used for the Z:P ratios.

ton are able to coexist on so few limiting resources: diversity can be easily increased by the addition of prey-or host-specific zooplankton and viral controls (Hutchinson 1961; Thingstad and Sakshaug 1990).

In this study we have explicitly resolved a grazer community with 30 different size classes of zooplankton. This "top-down" grazer control, coupled to the size-dependent "bottom-up" nutrient controls, allows the model to produce a realistic global size distribution (Thingstad and Sakshaug 1990; Armstrong 1994). The smallest and most competitive phytoplankton groups are kept under control by the smallest zooplankton, allowing larger size classes to become established when excess nutrients are available. The importance of this mechanism can be demonstrated by removing predator–prey specificity. If the modeled zooplankton are allowed to graze equally on all phytoplankton, the entire system of diversity collapses, leading to the exclusion of all but one or two very small size classes (Fig. 8c,d). This result demonstrates the importance of top-down controls in maintaining the size structure and taxonomic diversity of marine communities. Furthermore, it shows that in this model, transient nutrient pulses alone are not enough to support populations of large cells over long timescales.

The global balance of top-down and bottom-up controls is explored further in Fig. 9. On the left-hand side, Fig. 9 shows the annual average physiological limitation of surface phytoplankton in three size classes. This is expressed as the realized fraction of the maximum growth rate at 20°C, which is equivalent to the combined nutrient-, light-, and temperature-limitation terms, as outlined in the Web Appendix, Eq. A16. Conversely, the right-hand side of Fig. 9 gives an approximation of the degree of top-down control on each size class, in the form of surface Z:P ratios. These are calculated by pairing zooplankton and phytoplankton in terms of optimal grazing preference. For example, picophytoplankton (diameter < 2 μm) are paired with all zooplankton with diameter < 20 μm.

Focusing initially on the picophytoplankton, Fig. 9a shows that physiological limitation of this size class is distributed as might be expected. On average, the highest growth rates are attained in upwelling and subpolar regions, whereas strong bottom-up limitation (as indicated by low values of the dimensionless growth limitation term) is seen in both the nutrient-depleted subtropical gyres and the cold and sometimes iron-limited polar regions. In a complementary fashion, Fig. 9b shows that the upwelling, subpolar, and polar regions are character-

ized by very high Z:P ratios ($\sim$ 10), suggesting strong top-down control, whereas the oligotrophic gyres have much lower ratios ($\sim$ 0.1). Taken together, the two figures suggest that within the smallest size class, the oligotrophic gyres are dominated by bottom-up controls (i.e., nutrient limitation), the upwelling and subpolar regions are dominated by top-down, grazing controls, and the high-latitude polar regions are subject to both strong bottom-up (i.e., light and temperature) limitation and intense grazing pressure.

Within the next largest size class, Fig. 9c shows that the nanophytoplankton reach a considerably lower fraction of their maximum growth rates than the picophytoplankton. This is primarily attributable to the decreased nutrient affinity of these larger cells (neither temperature limitation nor relative light limitation scale with size in the model; Table 2). The slower relative growth of the nanophytoplankton supports a smaller grazer community, and results in weaker top-down control. This is shown in Fig. 9d, where global Z:P ratios are predominantly < 1 outside of upwelling and coastal regions.

Finally, the largest size class, the microphytoplankton, shows the lowest relative growth rates (Fig. 9e) and the lowest Z:P ratios. The very low nutrient affinities within this size class result in strong nutrient limitation, and the associated slow growth rates are unable to support a large grazer community, leading to weak top-down control.

The highlighted patterns are consistent with the view that strong top-down control limits the abundance of the smallest and fastest-growing phytoplankton, whereas bottom-up controls place limits on the number of size classes that are able to coexist (Armstrong 1994). The results presented in Fig. 9 additionally suggest that the observed shift from low to high Z:P ratios with increased productivity and total biomass seen in Fig. 5 (and Gasol et al. 1997) is driven by an increasing fraction of the community coming under strong top-down control.

Parameterizing complexity—The field of marine ecosystem and biogeochemical modeling is currently faced with two important and conflicting challenges. Firstly, the marine ecosystem is complex, and models that begin to resolve this complexity contain a large number of parameters that are often poorly constrained by observations. Secondly, even the most complex models are based on highly aggregated representations of functionally diverse species, and these are rarely general enough to perform well across large environmental gradients. Recent studies have begun to address these problems by focusing on the more general rules that govern complexity and diversity, rather than by trying to quantify and parameterize the diversity itself. A major advantage of these "self-organizing" models (Follows et al. 2007), is that they are able to resolve greater ecological complexity with fewer specified parameters.

One of the main challenges of this approach is to identify the general rules or trade-offs that govern competition between organisms (Litchman et al. 2007). Plankton physiological and ecological parameters have been linked to community structure through a number of different mechanisms (Armstrong 1994; Irwin et al. 2006), but here the trade-offs are constrained using well-known relationships between organism size and metabolic rates (Moloney and Field 1991; Tang 1995; Hansen et al. 1997).

We have developed a model using observed physiological and ecological relationships with cell size. The model begins to resolve the internal cellular physiology (Geider et al. 1998) of a diverse community of phytoplankton and their zooplankton grazers. The model produces qualitatively realistic results in terms of broad global distributions of nutrients, biomass, and primary productivity, and captures known ecological trends, such as the increasing coexistence of large size classes in more productive regions, and higher Z:P ratios in coastal and upwelling regions. Using this model we are able to clarify the mechanisms that underpin the size structure of marine communities at a global scale, and we have highlighted the importance of both nutrient and grazer controls in shaping these ecosystems.

In summary, the size dependence of key phytoplankton parameters, particularly those relating to nutrient affinity, gives small phytoplankton a significant competitive advantage over large cells. In the absence of top-down controls, small cells would dominate marine communities, but the inclusion of many zooplankton types allows much greater coexistence of larger cells through the kill-the-winner mechanism. The combined effects of bottom-up and top-down controls thus underpin the observed global size structure of marine communities. The model is therefore well suited to address important questions regarding the links between marine physiology, ecology, biogeography, and biogeochemistry.

References

ARMSTRONG, R. A. 1994. Grazing limitation and nutrient limitation in marine ecosystems: Steady state solutions of an ecosystem model with multiple food chains. Limnol. Oceanogr. **39:** 597–608, doi:10.4319/lo.1994.39.3.0597

———. 2003. A hybrid spectral representation of phytoplankton growth and zooplankton response: The "control rod" model of plankton interaction. Deep-Sea Res. II **50:** 2895–2916, doi:10.1016/j.dsr.2003.07.003

BAIRD, M. E., AND I. M. SUTHERS. 2007. A size-resolved pelagic ecosystem model. Ecol. Model. **203:** 185–203, doi:10.1016/j.ecolmodel.2006.11.025

BANAS, N. 2011. Adding complex trophic interactions to a size-spectral plankton model: Emergent diversity patterns and limits on predictability. Ecol. Model. **222:** 2663–2675, doi:10.1016/j.ecolmodel.2011.05.018

BEHRENFELD, M. J., AND P. G. FALKOWSKI. 1997. Photosynthetic rates derived from satellite-based chlorophyll concentration. Limnol. Oceanogr. **42:** 1–20, doi:10.4319/lo.1997.42.1.0001

BOYD, P. W., AND M. J. ELLWOOD. 2010. The biogeochemical cycle of iron in the ocean. Nature Geosci. **3:** 675–682, doi:10.1038/ngeo964

CARR, M.-E., AND OTHERS. 2006. A comparison of global estimates of marine primary production from ocean color. Deep-Sea Res. II **53:** 541–770, doi:10.1016/j.dsr2.2006.01.028

CAVENDER-BARES, K. K., A. RINALDO, AND S. W. CHISHOLM. 2001. Microbial size spectra from natural and nutrient enriched ecosystems. Limnol. Oceanogr. **46:** 778–789, doi:10.4319/lo.2001.46.4.0778

CERMEÑO, P., E. MARAÑÓN, D. HARBOUR, AND R. P. HARRIS. 2006. Invariant scaling of phytoplankton abundance and cell size in contrasting marine environments. Ecol. Lett. **9:** 1210–1215, doi:10.1111/j.1461-0248.2006.00973.x

CHISHOLM, S. W. 1992. Phytoplankton size, p. 213–237. *In* P. G. Falkowski and A. D. Woodhead [eds.], Primary productivity and biogeochemical cycles in the sea. Plenum.

CONKRIGHT, M. E., H. E. GARCIA, T. D. O'BRIEN, R. A. LORCANINI, T. P. BOYER, C. STEPHENS, AND J. I. ANTONOV. 2002. World Ocean Atlas 2001, v. 4, Nutrients. NOAA Atlas NESDIS52.

DROOP, M. R. 1968. Vitamin B12 and marine ecology, IV. The kinetics of uptake, growth and inhibition in *Monochrysis lutheri*. J. Mar. Biol. Assoc. U.K. **48:** 689–733, doi:10.1017/S0025315400019238

DUTKIEWICZ, S., B. A. WARD, F. M. MONTEIRO, AND M. J. FOLLOWS. 2012. Interconnection of nitrogen fixers and iron in the Pacific Ocean: Theory and numerical simulations. Global Biogeochem. Cycles **26:** GB1012, doi:10.1029/2011GB004039

FINKEL, Z. V. 2001. Light absorption and size scaling of light-limited metabolism in marine diatoms. Limnol. Oceanogr. **46:** 86–94, doi:10.4319/lo.2001.46.1.0086

FOLLOWS, M. J., S. DUTKIEWICZ, S. GRANT, AND S. W. CHISHOLM. 2007. Emergent biogeography of microbial communities in a model ocean. Science **315:** 1843–1846, doi:10.1126/science.1138544

GASOL, J. M., P. A. DEL GIORGIO, AND C. M. DUARTE. 1997. Biomass distribution in marine planktonic communities. Limnol. Oceanogr. **42:** 1353–1363, doi:10.4319/lo.1997.42.6.1353

GEIDER, R. J., H. L. MACINTYRE, AND T. M. KANA. 1998. A dynamic regulatory model of phytoacclimation to light, nutrients and temperature. Limnol. Oceanogr. **43:** 679–694, doi:10.4319/lo.1998.43.4.0679

GENTLEMAN, W. C., A. LEISING, B. FROST, S. STROM, AND J. MURRAY. 2003. Functional responses for zooplankton feeding on multiple resources: A review of assumptions and biological dynamics. Deep-Sea Res. II **50:** 2847–2875, doi:10.1016/j.dsr2.2003.07.001

HANSEN, P. J., P. K. BJØRNSEN, AND B. W. HANSEN. 1997. Zooplankton grazing and growth: Scaling with the 2–2000-μm body size range. Limnol. Oceanogr. **42:** 678–704, doi:10.4319/lo.1997.42.4.0687

HIRATA, T., AND OTHERS. 2011. Synoptic relationships between surface chlorophyll-*a* and diagnostic pigments specific to phytoplankton functional types. Biogeosciences **8:** 311–327, doi:10.5194/bg-8-311-2011

HOOD, R. R., AND OTHERS. 2006. Pelagic functional group modelling: Progress, challenges and prospects. Deep-Sea Res. II **53:** 459–512, doi:10.1016/j.dsr2.2006.01.025

HUTCHINSON, G. E. 1961. The paradox of the plankton. Am. Nat. **95:** 137–145, 882, doi:10.1086/282171

IRWIN, A. J., Z. V. FINKEL, O. M. E. SCHOFIELD, AND P. G. FALKOWSKI. 2006. Scaling up from nutrient physiology to the size-structure of phytoplankton communities. J. Plankton Res. **28:** 459–471, doi:10.1093/plankt/fbi148

KIØRBOE, T. 2008. A mechanistic approach to plankton ecology. Princeton Univ. Press.

KLEYPAS, J. A., AND S. C. DONEY. 2001. Nutrients, chlorophyll, primary production and related biogeochemical properties in the ocean mixed layer. A compilation of data collected at nine JGOFS sites [Internet]. Available from http://dss.ucar.edu/datasets/ds259.0/

KOSTADINOV, T. S., D. A. SIEGEL, AND S. MARITORENA. 2009. Retrieval of the particle size distribution from satellite ocean color observations. J. Geophys. Res. **114:** C09015, doi:10.1029/2009JC005303

KRIEST, I., AND A. OSCHLIES. 2007. Modelling the effect of cell-size-dependent nutrient uptake and exudation on phytoplankton size spectra. Deep-Sea Res. I **54:** 1593–1618, doi:10.1016/j.dsr.2007.04.017

LAWS, E. A. 1975. The importance of respiration losses in controlling the size distribution of marine phytoplankton. Ecology **56:** 419–426, doi:10.2307/1934972

LITCHMAN, E., C. A. KLAUSMEIER, O. M. SCHOFIELD, AND P. G. FALKOWSKI. 2007. The role of functional traits and trade-offs in structuring phytoplankton communities: Scaling from cellular to ecosystem level. Ecol. Lett. **10:** 1170–1181, doi:10.1111/j.1461-0248.2007.01117.x

MENDEN-DEUER, S., AND E. J. LESSARD. 2000. Carbon to volume relationships for dinoflagellates, diatoms, and other protist plankton. Limnol. Oceanogr. **45:** 569–579, doi:10.4319/lo.2000.45.3.0569

MOLONEY, C. L., AND J. G. FIELD. 1991. The size-based dynamics of plankton food-webs. I. A simulation model of carbon and nitrogen flows. J. Plankton Res. **13:** 1003–1038, doi:10.1093/plankt/13.5.1003

MONGIN, M., D. M. NELSON, P. PONDAVEN, AND P. TRÉGUER. 2006. Simulation of upper-ocean biogeochemistry with a flexible-composition phytoplankton model: C, N and Si cycling and Fe limitation in the Southern Ocean. Deep-Sea Res. II **53:** 601–619, doi:10.1016/j.dsr2.2006.01.021

MONTAGNES, D. J. S., AND D. J. FRANKLIN. 2001. Effect of temperature on diatom volume, growth rate, and carbon and nitrogen content: Reconsidering some paradigms. Limnol. Oceanogr. **46:** 2008–2018, doi:10.4319/lo.2001.46.8.2008

MOORE, J. K., S. C. DONEY, J. A. KLEYPAS, D. M. GLOVER, AND I. Y. FUNG. 2002. An intermediate complexity marine ecosystem model for the global domain. Deep-Sea Res. II **49:** 403–462, doi:10.1016/S0967-0645(01)00108-4

RAIMBAULT, P., M. RODIER, AND I. TAUPIER-LETAGE. 1988. Size fraction of phytoplankton in the Ligurian Sea and the Algerian Basin (Mediterranean Sea): Size distribution versus total concentration. Mar. Microb. Food Webs **3:** 1–7.

RAVEN, J. A. 1998. The twelfth Tansley Lecture. Small is beautiful: The picophytoplankton. Funct. Ecol. **12:** 503–513, doi:10.1046/j.1365-2435.1998.00233.x

SCHARTAU, M., M. R. LANDRY, AND R. A. ARMSTRONG. 2010. Density estimation of plankton size spectra: A reanalysis of IronEx II data. J. Plankton Res. **32:** 1167–1184, doi:10.1093/plankt/fbq072

SHELDON, R. W., A. PRAKASH, AND W. H. SUTCLIFFE, JR. 1972. The size distribution of particles in the ocean. Limnol. Oceanogr. **17:** 327–340, doi:10.4319/lo.1972.17.3.0327

STOCK, C. A., T. M. POWELL, AND S. A. LEVIN. 2008. Bottom-up and top-down forcing in a simple size-structured plankton dynamics model. J. Mar. Syst. **74:** 134–152, doi:10.1016/j.jmarsys.2007.12.004

SUTTLE, C. A. 2007. Marine viruses—major players in the global ecosystem. Nat. Rev. Microbiol. **5:** 801–812, doi:10.1038/nrmicro1750

TANG, E. P. Y. 1995. The allometry of algal growth and respiration. Master's thesis. McGill Univ.

TAYLOR, A. G., M. R. LANDRY, K. E. SELPH, AND E. J. YANG. 2011. Biomass, size structure and depth distributions of the microbial community in the eastern equatorial Pacific. Deep-Sea Res. II **58:** 342–357, doi:10.1016/j.dsr2.2010.08.017

THINGSTAD, T. F., AND R. LIGNELL. 1997. Theoretical models for the control of bacterial growth rate, abundance, diversity and carbon demand. Aquat. Microb. Ecol. **13:** 19–27, doi:10.3354/ame013019

———, AND E. SAKSHAUG. 1990. Control of phytoplankton growth in nutrient recycling ecosystems. Theory and terminology. Mar. Ecol. Prog. Ser. **63:** 261–272, doi:10.3354/meps063261

WUNSCH, C., AND P. HEIMBACH. 2007. Practical global ocean state estimation. Physica D **230:** 197–208, doi:10.1016/j.physd.2006.09.040

Joint Program Reprints are available free of charge (limited quantities). To order: please use contact information on inside of front cover.

2012-37 Global emission estimates and radiative impact of C_4F_{10}, C_5F_{12}, C_6F_{14}, C_7F_{16}, C_8F_{18}, Ivy, D.J., M. Rigby, M. Baasandorj, J.B. Burkholder and R.J. Prinn, *Atmospheric Chemistry and Physics*, 12: 7635–7645 (2012)

2012-38 Global and regional emission estimates for HCFC-22, Saikawa, E., M. Rigby, R.G. Prinn, S.A. Montzka, B.R. Miller, L.J.M. Kuijpers, P.J.B. Fraser, M.K. Vollmer, T. Saito, Y. Yokouchi, C.M. Harth, J. Mühle, R.F. Weiss, P.K. Salameh, J. Kim, S. Li, S. Park, K.-R. Kim, D. Young, S. O'Doherty, P.G. Simmonds, A. McCulloch, P.B. Krummel, L.P. Steele, C. Lunder, O. Hermansen, M. Maione, J. Arduini, B. Yao, L.X. Zhou, H.J. Wang, J.W. Elkins and B. Hall, *Atmospheric Chemistry and Physics*, 12: 10033–10050 (2012)

2012-39 Flexible NOx Abatement from Power Plants in the Eastern United States, Sun, L., M. Webster, G. McGaughey, E.C. McDonald-Buller, T. Thompson, R. Prinn, A.D. Ellerman and D.T. Allen, *Environmental Science & Technology*, 46(10): 5607–5615 (2012)

2012-40 A size-structured food-web model for the global ocean, Ward, B.A., S. Dutkiewicz, O. Jahn and M.J. Follows, *Limnology and Oceanography*, 57(6): 188–1891 (2012)

2013-1 The Impact of Climate Policy on US Aviation, Winchester, Niven, Christoph Wollersheim, Regina Clewlow, Nicholas C. Jost, Sergey Paltsev, John M. Reilly and Ian A. Waitz, *Journal of Transport Economics and Policy*, 47(1): 1–15 (2013)

2013-2 Impact of anthropogenic absorbing aerosols on clouds and precipitation: A review of recent progresses, Wang, Chien, *Atmoshperic Research*, 122: 237–249 (2013)

2013-3 Applying engineering and fleet detail to represent passenger vehicle transport in a computable general equilibrium model, Karplus, Valerie, Sergey Paltsev, Mustafa Babiker and John M. Reilly, *Economic Modelling,* 30: 295–305 (2013)

2013-4 Should a vehicle fuel economy standard be combined with an economy-wide greenhouse gas emissions constraint? Implications for energy and climate policy in the United States, Karplus, Valerie, Sergey Paltsev, Mustafa Babiker and John M. Reilly, *Energy Economics*, 36: 322–333 (2013)

2013-5 Climate impacts of a large-scale biofuels expansion, Hallgren, W., C.A. Schlosser, E. Monier, D. Kicklighter, A. Sokolov and J. Melillo, *Geophysical Research Letters*, 40(8): 1624–1630 (2013)

2013-6 Non-nuclear, low-carbon, or both? The case of Taiwan, Chen, Y.-H.H., *Energy Economics*, 39: 53–65 (2013)

2013-7 The Cost of Adapting to Climate Change in Ethiopia: Sector-Wise and Macro-Economic Estimates, Robinson, S., K. Strzepek and Raffaello Cervigni, *IFPRI ESSP WP 53* (2013)

2013-8 Historical and Idealized climate model experiments: an intercomparison of Earth system models of intermediate complexity, Eby, M., A.J. Weaver, K. Alexander, K. Zickfield, A. Abe-Ouchi, A.A. Cimatoribus, E. Crespin, S.S. Drijfhout, N.R. Edwards, A.V. Eliseev, G. Feulner, T. Fichefet, C.E. Forest, H. Goosse, P.B. Holden, F. Joos, M. Kawamiya, D. Kicklighter, H. Kiernert, M. Matsumoto, I.I. Mokov, E. Monier, S.M. Olsen, J.O.P. Pedersen, M. Perrette, G. Phillpon-Berthier, A. Ridgwell, A Schlosser, T. Schneider von Deimling, G. Shaffer, R.S. Smith, R. Spahni, A.P. Sokolov, M. Steinacher, K. Tachiiri, K. Tokos, M. Yoshimori, N Zeng and F. Zhao, *Clim. Past*, 9:1111–1140 (2013)

2013-9 Correction to "Sensitivity of distributions of climate system properties to the surface temperature data set", and Sensitivity of distributions of climate system properties to the surface temperature data set, Libardoni, A.G. and C.E. Forest, *Geophysical Research Letters*, 40(10): 2309–2311 (2013), and 38(22): 1–6 (2011)

2013-10 Permafrost degradation and methane: low risk of biogeochemical climate-warming feedback, Gao, Xiang, C. Adam Schlosser, Andrei Sokolov, Katey Walter Anthony, Qianlai Zhuang and David Kicklighter, *Environmental Research Letters*, 8(3): 035014 (2013)

For a complete list of titles see:
http://globalchange.mit.edu/research/publications/reprints